COMPUTER AIDED DESIGN OF A HOMOPOLAR LINEAR SYNCHRONOUS MOTOR DRIVEN LEVITATED ELECTRICAL TRANSPORT VEHICLES

تصميم محرك تزامنى خطى متجانس الأقطاب لرفع وجر مركبات النقل الكهربية باستخدام الحاسب الآلى

S.A EL-Drieny

Electrical Engineering Department, Faculty Of Engineering, EL-Mansoura University, EL-Mansoura, Egypt

ملخص البحث

انضم حديثاً المحرك التزامنى الخطى متجانس الأقطاب إلى مجموعة المحركات الخطية القادرة على تزويد مركبات النقل الكهربية بكل من قوتى الرفع والجر الكهربى. من المعروف أن المشاكل التى تواجه استخدام مثل هذا النوع من المحركات الخطية فى رفع وجر المركبات الكهربية هى: ١-عدم توافق وتزامن كل من قوتى الرفع والجر الكهربى أثناء كل فترة زمنية من دورة التشغيل المقترحة للمركبة الكهربية وبناء عليه فإنه لتحقيق هذا التوافق يلزم حساب كل من كثافة الفيض المغناطيسى ، الشكل الهندسى للأقطاب ، زوايا الحمل ومعامل القدرة بدقة .٢- يعمل المحرك التزامنى فقط عند سرعة التزامن عندما يغذى من مصدر ثابت التردد. والحصول على سرعات متغيرة تتفق مع دورة التشغيل فإنه يلزم تغذية المحرك من مصدر للتيار متغير التردد مع وجوده فى دائرة تحكم مغلقة وعليه فإنه يجب تزويد دائرة التحكم بزوايا تشغيل مناسبة لكل فترة زمنية من دورة التشغيل. .

يقدم البحث أسلوباً لتصميم مثل هذا النوع من المحركات مستخدماً الحاسب الآلى ويعتمد هذا الأسلوب على البنود التالية: ١-.تمثيل أداء الآلة بالمخطط الاتجاهى . ٢-إختيار زاوية التشغيل ٣-تطبيق المخطط الانسيابى المقترح لخطوات التصميم.

كتب المخطط الأنسيابى فى شكل برنامج للحاسب الآلى للوصول إلى تحقيق تزامن لكل من قوتى الرفع والجر المناظرة لزوايا الحمل ومعامل القدرة وفى حالة ما إذا كانت هذه القوى غير مناسبة لدورة التشغيل المقترحة للمحرك يتم افتراض زوايا أخرى للحمل وطول الفترة الهوائيةوأبعاد المحرك وتعاد الخطوات السابقة وصولاً إلىتحقيق التزامن والتوافق لقوى الجر والرفع مع القيم المناظرة لزوايا الحمل والقدرة.

ولقد تم تطبيق هذا الأسلوب لتصميم محرك تزامنى خطى لرفع وجر مركبة كهربية وزنها ٣ طن وتتحرك بسرعة ٣٦ ك.م/ساعة بعجلة مقدارها ١.٤٧ متر/(ثانية)^2

والبحث يقدم أسلوباً مرناً مساعداً فى يدى مصممى مثل هذا النوع من المحركات تمكنهم من الأخذ فى الاعتبار العديد من متغيرات التصميم وظروف التشغيل.

Accepted 29 December 1996

Abstract

Recently, the E core homopolar linear synchronous motor HLSM has been introduced to the family of linear motors capable of exerting both traction and attraction forces. The HLSM is preferred for use in driving and levitating electrical transport vehicles due to the advantage of combined traction and attraction forces. The usual problems of this application are: (i) The synchronization of exact traction force with the correct attraction force at all times of duty cycle of transport vehicle. Hence, the correct air-gap flux density, air-gap length, geometry of rail track pole and identification of operating conditions which meet the traction and attraction forces requirements should be properly determined. (ii) The HLSM operates only at synchronous speed. To obtain variable speeds operation, the HLSM must be fed by current source inverter and must be operated under closed-loop control circuit. Under this operation it is possible to select the operating angle between the direct-axis and armature current. The phasor diagram representing the performance of HLSM depends mainly on this angle.

This paper presents a design technique of a linear synchronous motor for traction and attraction of electrical transport vehicles .The design technique is based on :

1) Representation of the motor performance using the phasor diagram to explore the interaction between the fields and the motor parameters such as direct and quadrature axes reactances, induced voltage in the armature due to field excitation only , power factor and power angle.
2) Selection of the operating angle when HLSM is fed by current source inverter and operated under closed-loop control circuit..Despite the variable reluctance construction of this motor the direct and quadrature axes reactances are more close together. So,it is possible to select an optimum value of operating angle for unity power factor designs. This choice caused a reduction of the effects of the armature reaction on the air gap flux density under the pole faces. In turn, this reduces saturation in the armature teeth, the most stressed part of the iron . In addition.,at the same time, this choice maximizes the thrust per unit area , and hence ,for a specified power output , tends to lead a minimum size of the motor. Consequently the (power / weight) ratio is maximized and this is one of the important aims for such application in transportation system
3) Application of the suggested design flow chart acts as a quick and simple tool to predict the attraction and traction forces and to examine the effects of varying the major dimensions of the motor.
4) Study the effect of air-gap length on the attraction and traction forces

The design technique is applied to design a HLSM for lifting a 3 ton vehicle at 36 Km/h speed and accelerates at 1.47 m/sec^2.

List of symbols:

A : The area of the air-gap.
b : Length of active conductors.
B' : RMS fundamental component of flux density in air-gap produced by terminal voltage. $= V_a / (\frac{C K_d K_p}{m}) V b$
B_a : RMS. fundamental component of flux density in air-gap produced by armature excitation $= \left(\frac{\mu_o \tau}{\pi g} \right) k_a$

Bf : RMS fundamental component of flux density in air-gap produced by field excitation

$$= \sqrt{2}\,\frac{\mu_o}{\pi}\,\frac{\sin\alpha}{g}\,N_f\,I_f$$

B_g . RMS. fundamental component of flux density in air-gap .
C : Total number of series connected conductors.
C_d . Direct-axis armature reactance coefficient = X_{ad} / X_m .
C_q : Quadrature-axis armature reactance coefficient = X_{aq} / X_m .
d : Distance from center of pole face.
E_f : RMS. fundamental voltage induced in armature due to field current only.
E_g : Voltage induced in armature by B_g.
g : effective air-gap length.
I_a . RMS. armature current.
I_f : D.C. current in the field winding.
I'_f . RMS. value of field current referred to armature.

K_a : RMS. armature surface current density = $\dfrac{Ck_dk_p}{2\tau.p}\,I_a$.

Kad: RMS direct-axis armature surface current density
Kaq: RMS quadrature-axis armature surface current density
K_d : Winding distribution factor.
K_p : Winding pitch factor.
l_p : Pole face width.
m : Number of phases.
N_f : Turns / pole in the field winding
p : Number of pole pairs.
P : Power.
t : Thrust per unit area of armature surface.
T . Total thrust..
V : The relative velocity between the armature and the polar structure
V_a : Terminal voltage of motor..
w_t . Tooth width.
W_{mp}. Magnetic energy per pole
Xm : Magnetizing reactance
Xl . Leakage reactance
X_{ad} . Direct-axis saturated armature reactance.
X_{aq} Quadrature-axis saturated armature reactance.
X_{af} : Saturated mutual reactance between armature and field.
α : Angular span of pole face = (π lp / 2τ).
μ_o . Permeability of free space $4\pi \times 10^{-7}$ H / m.
τ : Pole pitch.
τ_s : Slot pitch.
ϕ,ϕ' : Phase angle between armature current and voltage or gap flux density,respectively .
λ Angle between q- axis and peak of K_a.
ψ :(Operating angle) between d-axis and peak of K_a.

1. Introduction :

Recently, a homopolar linear synchronous motor is used for electrical transport vehicles because it provides both traction and attraction forces. The problems associated with new transport system are :

1) The linear synchronous motor LSM has no variable speed capability when energized from a fixed frequency supply, and hence requires a variable frequency supply to be of practical use.[6,8].
2) If the equipment which controls the attraction force fails, to a condition of maximum force, it will produce a large amount of braking force.
3) With an active vehicle system, the vehicle carries several motors with their power conversion and control equipment which act as extra load on the vehicle's attraction system.

When the LSM is used to combine traction and attraction forces, the thrust necessary to accelerate the vehicle and to satisfy the duty cycle must also be achieved at appropriate values of speed and frequency. Hence a power converter is required to feed the armature winding of LSM with current at not only the correct frequency but also at the load angle which will produce the necessary thrust. Furthermore, a fast chopper is necessary to control the field current and to adjust the levitation force to match the vehicle load [11,12].

This paper presents the solution for some of the previous problems by introducing a design technique based on (i) representation of phasor diagram which represents the HLSM performance.(ii) application of both the suggested flow chart design and the given control system A sketch of idealized LSM is shown in figure (1). The block diagram of control system is shown in figure(2) and is divided into two parts : the left hand controls the speed and maintains the current at fixed value . While the right hand controls the phase angle ψ This is accomplished by detecting the phase angle between two wave shapes of the same frequency the signal from the pole-position sensor and the voltage-wave which controls the inverter frequency

2. General Design Idea

The design of an electrical machine is usually carried out by trial and error. Firstly; the designer chooses the geometry, the dimensions, the magnetic and electric loading and then determines the performance and parameters of the machines. These steps are iterated until the design specifications are met.

Although ,the modern computers allow the design processes to be carried out very fast, both the optimization of the design and the previous experience with similar motors are very essential.

When dealing with a novel application, it is more convenient to start directly with the design specifications, express them in terms of electric and magnetic loadings, choosing the suitable geometry, and finally determine the dimensions. This approach was adopted for the design of HLSM. Design flow chart based on choosing the values of specific magnetic and electric loadings by trial and error until design becomes practical is shown in figure (9).

In this motor, the field and armature windings lie in planes perpendicular to one another as shown in figure (1). As a result, the magnetic circuit path for the constant homopolar flux is transverse to direction of motion. In contrast, the fundamental component of the alternating flux, partly is generated by salient pole, variable-reluctance construction, and partly by the time-varying armature currents, develops longitudinally flux to the direction of motion. The ferromagnetic material of the HLSM armature carries a flux density which varies along the armature winding air

-gap between $+\hat{B}$ and $-\check{B}$ (i.e. around an average value) instead of between positive $+\hat{B}$ and $-\hat{B}$ (and negative peaks. as in heteropolar synchronous machines.

Since, an average component of flux density, B, in addition to the useful alternating component, are presented in the air gap, the designer has to push the armature teeth and most of armature iron into saturation. On the other hand, since the motor relies on variable reluctance effects for its operation, saturation of the track poles structure cannot be allowed. The steady-state performance can be predicted according to conventional two-reaction theory [2,3] and represented in the phasor diagram of figure (3). An expression of the output power[4] can easily be derived and is given by :

$$P = m \left(X_{ad} I_f I_a \cos \psi - \frac{X_{ad} - X_{aq}}{2} I_a^2 \sin 2\Psi \right) \qquad (1)$$

In the homopolar LSM, the pole pitch is half the distance between two adjacent poles . Hence the saturated reactance X_{aq} can be made equal to X_{ad} by choosing the pole face length to be smallera than the pole pitch lenght. In general, the difference between X_{ad} and X_{aq} is relatively small, so that the first part of the power equation P is substantially larger than the second. It appears, for given field and armature currents, the output is a maximum when $\Psi = 0$, as in d.c. machines.

Several considerations, however, act against the design choice $\psi \leq 0$. Firstly; in this region, the armature current lags behind the voltage and, hence, the KVA rating of both the machine and its inverter exceeds the KW rating. A leading voltage, also, prevents the commutation of the switching elements. Secondly; the attention on the currents is misleading, since the machine output is not limited by the dissipation of heat resulting from ohmic losses. As was mentioned before, the machine is brought to saturation of the magnetic flux path. For the case of $\psi \leq 0$, the fundamental components of both the armature and field flux densities (B_a and B_f), or more precisely, their mmf's, add up over at least half of the pole face, thus compounding the problem of iron saturation. figure (4) shows how this difficulty may be solved by choosing a positive value of Ψ.

3. Design Arrangement of HLSM :

The starting point of early stage of desiguing such type of motor have to be considered as follows :

1) The maximum permissible flux density on the pole face $B_{pf(max)}$
2) The maximum allowable flux density in the armature teeth $B_{t(max)}$.

When the teeth are not saturated, the above flux densities are related by

$$B_{t(max)} = \frac{\tau_s}{w_t} B_{pf(max)} \qquad (2)$$

To estimate the air-gap flux density B_g the following flux densities must be firstly considered

The two fundamental components of flux density produced by armature windings are given by

$$B_{ad} = C_d \frac{\mu_o \tau}{\pi g} K_{ad}$$

$$B_{aq} = C_q \frac{\mu_o \tau}{\pi g} K_{aq} \qquad (3)$$

The fundamental of flux density [3] produced by field excitation is given by

$$B_f = \frac{2}{\pi} \cdot \frac{\mu_o}{\sqrt{2}} \cdot \frac{\sin\alpha}{g} N_f \cdot I_f \qquad (4)$$

The total flux density wave B_g is the sum of B_f, B_{ad}, and B_{aq}, as shown in figure (5). In the design stage, the electrical and magnetic loadings K_a and B_g are specified; the phasor diagram is then used to determine B_f and hence the required field excitation $N_f . I_f$. A difficulty, however, arises, since the angle Ψ is not known early. This difficulty can be solved by using the construction of figure (6) where the angle Ψ is determined by drawing a segment equal to $(B_{aq} / \cos\Psi) = (\mu_o \tau / \pi g) C_q K_a$ in the direction perpendicular to K_a. The field flux density B_f is then found as shown in figure (7).The preceeding analysis doesn't take into account the effect of leakage fluxes such as slot leakage flux and the over hang leakage flux. To account for the overall effect of these fluxes [5] an appropriate parameter X_l (leakage reactance) must be considered consequently, the phasor diagram will be modified as shown in figure (8). Insight may be gained into the relation between the electric and the magnetic loadings and the design parameters by normalizing this modified phasor diagram ,so, as to put into evidence the magnetic field quantities. Particularly simple analytical expressions are obtained in case of practical interest, when the machine is designed for unity power factor and when the armature resistance is neglected. The following expressions can be obtained :

$$B_a = \frac{\mu_o \tau}{\pi g} K_a \qquad (5)$$

$$X_m = \frac{\mu_o b V \left(C K_d K_p\right)^2}{2\pi p m g} \qquad (6)$$

$$B' = \frac{V_a}{\left(C K_d K_p / m\right) b V} \qquad (7)$$

$$K_a = \frac{C K_d K_p}{2 p \tau} I_a \qquad (8)$$

$$\overline{ob} = \left(\frac{X_l}{X_m} + C_q\right) \cdot \frac{\mu_o \tau}{\pi g} \frac{1}{\sin\Psi} K_a = B_f - \left(C_d - C_q\right) \frac{\mu_o \tau}{\pi g} K_a \sin\Psi \qquad (9)$$

and solving for K_a,

$$K_a = \frac{\pi g}{\mu_o \tau} \frac{B_f}{\left(C_d - C_q\right) \sin\Psi + \left(\frac{X_l}{X_m} + C_q\right) \frac{1}{\sin\Psi}} \qquad (10)$$

A relation is thus established between K_a and B_f which are indices of the electric and magnetic loadings, respectively.

4. Forces Calculation :

To calculate the forces, the energy stored in the magnetic field must be evaluated, and take negative of its derivative with respect to the direction of the desired component. The magnetic energy stored in the air-gap over one pole pitch is given by [9, 10, 11, 12].

$$W_{mp} = \frac{\mu_o}{2} \int_{-l_p/2}^{+l_p/2} \left(H_f + H_a\right)^2 b.g.dx$$

$$= \frac{\mu_o}{2} \frac{b}{g} \int_{-l_p/2}^{+l_p/2} \left[N_f I_f + \sqrt{2}\,\frac{\tau}{\pi} K_a \cos\left(\frac{\pi}{\tau}x + \lambda\right)\right]^2 dx$$

$$= \frac{\mu_o}{2} \frac{b}{g} \left[\begin{array}{l} \left(N_f I_f\right)^2 l_p + 4\sqrt{2}\, N_f I_f \left(\frac{\tau}{\pi}\right)^2 K_a \cos\lambda \sin\alpha + \\ 2\left(\frac{\tau}{\pi}\right)^2 K_a^2 \left(\frac{l_p}{2} + \frac{\tau}{2\pi}\cos 2\lambda \sin 2\alpha\right) \end{array} \right] \qquad (11)$$

where,

$\lambda = 90 - \Psi$

The total thrust over 2p poles is then $T = 2p \frac{\partial W_{mp}}{\partial x}$ and it can be given as

$$T = p\mu_o \frac{b}{g}\frac{\tau}{\pi} K_a \left[4\sqrt{2} N_f I_f \sin\lambda \sin\alpha - 2\frac{\tau}{\pi} K_a \sin 2\lambda \sin 2\alpha \right] \qquad (12)$$

and the total normal force under the armature is,

$$F_{ma} = 2P \frac{\partial W_{mp}}{\partial g} \qquad \text{or.}$$

$$F_{ma} = p\mu_o \frac{b}{g^2} \left[\begin{array}{l} \left(N_f I_f\right)^2 I_p - 4\sqrt{2} N_f I_f \left(\frac{\tau}{\pi}\right)^2 K_a \cos\lambda \sin\alpha + \\ 2\left(\frac{\tau}{\pi}\right)^2 K_a^2 \left(\frac{I_p}{2}\right) + \frac{\tau}{2\pi}\cos 2\lambda \sin 2\alpha \end{array} \right] \qquad (13)$$

In addition, in case of HLSM, there exists a normal force contributed by the feet under the field yoke.

$$F_{of} = \frac{1}{2}\frac{B_f^2}{\mu_o} A_f \qquad (14)$$

where, B_f is the flux density under the feet and A_f their area. The thrust force can be evaluated by another way as follows :

The electromagnetic force developed per unit area of the air-gap is

$$t = \frac{\text{power}}{A.V} = K_a B_g \cos\phi' = K_a \overline{ob} \cos\Psi \qquad (15)$$

The terms C_d and C_q are proportional to the direct and quadrature saturated reactances, and their difference is presented in equation (10). The approximation is now made that the first term in

the denominator, $(C_d - C_q)\sin\Psi$, is small in comparison with the second. This permits the following simplified expression for the thrust per unit area to be obtained when equations (9) and (10) are substituted into equation (15)

$$t \approx \frac{\pi g}{\mu_o \tau} \frac{B_f^2}{\frac{X_l}{X_m} + C_q} \frac{\sin 2\Psi}{2} \tag{16}$$

The force density is maximum for $\Psi = 45°$.

5. Forces Behavior :

There are many factors affecting on the forces behavior, the most important one which is considered in this paper is the air-gap length . This is considered as following :

The phasor diagram which is corresponding to ideal HLSM, no leakage reactance, unity power factor and angular span of pole face equal $\pi/2$, is shown in figure (4). From this phasor diagram and from equation (4), the following relations are considered :

$$\cos\lambda = K_a / K_f \tag{17}$$

where,

$$K_f = \frac{\sqrt{2}\, N_f I_f}{\tau} \sin\alpha = \frac{\sqrt{2}\, N_f I_f}{\tau} \tag{18}$$

And,

$$\sin\lambda = \frac{\pi}{\mu_o \tau} \frac{B_g}{K_f} \tag{19}$$

$$K_f^2 = \left(\frac{\pi g}{\mu_o \tau}\right)^2 B_g^2 + \frac{K_a^2}{4}$$

$$K_f = \frac{\pi g}{\mu_o \tau} \sqrt{B_g^2 + \left(\frac{\mu_o \tau}{2\pi g} K_a\right)^2} \tag{20}$$

The ratio of field to armature excitation is given by.

$$R = \frac{\pi}{2} \frac{K_f}{K_a} \frac{1}{\sin\alpha} = \frac{\pi N_f I_f}{\sqrt{2}\, \tau K_a} \tag{21}$$

From equation (12) and equation (13) the ratio of normal force to thrust is given.

$$\frac{F_n}{t} = \frac{\tau}{g} \frac{\frac{\pi}{2} + 4R\cos\lambda + \pi R^2}{4\pi R \sin\lambda}$$

$$\frac{F_n}{t} = \frac{\pi^2}{4} \frac{\frac{B_g^2}{2\mu_o} + \frac{\mu_o \tau}{\pi^2 g^2} \frac{K_a^2}{4}\left(\frac{1}{2} - \frac{4}{\pi^2}\right)}{B_g K_a} \tag{22}$$

Since $B_g K_s = t$ is independent of $\frac{\tau}{g}$, it is concluded that F_n depends on the air-gap length only through the ratio $\frac{\tau}{g}$

6. Numerical Example :

A design technique is applied for a wide range of operating angle ψ to design HLSM C-core type capable for driving and levitating (as a one of four similar motors intended for mounting at the corners) a 3 ton vehicle, 10 m/sec with acceleration of 1.47 m/sec^2. The airgap of this design was 10 mm the design steps are essentially iterative with the designer using trial values and subsequent refinements to bring it to an acceptable solution. It is outlined in flow chart of Fig. (9). The loop involves the fundamental design calculations for dimensions and weight. It is concerned with a virtually trial and error assessment of the design under different operating condition indicated by choices of ψ and φ'. The predicted performance is given as follows:

Rail clearance	10 mm	Thrust	1140 N
Power factor	1	Attractive force	7500 N
Weight/output power	13 kg/kW	Total weight	146 Kg
Efficiency	86%		

And the design data for one motor is given as follows :

Armature

Pole pitch	20 cm	coil span factor	0.866
slot pitch	22.2 mm	Chorded coil span	2/3 rd of pole pitch
No. of coils/phase	15	Winding factor	0.827
No. of turns/coil	58 turns	a.c packing factor	0.6
rated current	15.8 Amp	Current density	4.5 A/mm^2
Conductors cross section	3.95 mm^2		

Field

Ampere Turns	17334 AT
current density	8.7 A/mm^2
Rated field current	87 Amp

7. Concluding Remarks :

The main conclusion of this paper presents a design technique of a homopolar linear synchronous motor for combining traction and normal force . It develops the phasor diagram which represents the performance of the motor to explore the interaction between the fields and the classical parameters X_d, X_q, E. power factor, excitation and power angle.

The following remarkable points are got from this paper:

1) The thrust per unit area is proportional to the ratio of gap length to pole pitch. (g/τ). This is balanced, however, by an equal dependence of (X_l / X_m) on (g/τ)
2) The normal force per unit area is proportional to angular pole spread (α), it will decrease as α is decreasing and also inversely proportional to air-gap length
3) If the load angle is set to a value equal to the angular pole spread angle, no additive mmf will be present, even at the leading pole edge. Hence, it is possible to satisfy nearly simultansouly the two criteria of maximum thrust per unit area (1) and zero additive mmf.
4) The chosen value of Ψ can also be maintained when the motor operates at reduced power level. In the case of constant field current (and hence constant B_f), a constant Ψ yields a leading current which eases the commutation process in the inverter.
5) The thrust per unit area is proportional to the square of the magnetic loading if the saturation is neglected.
6) Appropriate pole-shaping increases the output by reducing C_q , which is an index of the permeane in the inter polar space
7) A smaller value of α will decrease the permeance of inter polar space, as will as the transverse flux, thus reducing the weight of the field yoke and the polar structure.

References.

[1] G.R Slemon, S.B Dewan "synchronous motor drive with current-source inverter"IEEE-IA-10, No.3. May 1974; PP 412-416.

[2] M. Kostenko, L. Piotrovsky "Electrical machines" Mir Publishers, Moscow, 1974 3rd Ed. vol.2.

[3] E.Levi and M.Panzer "Electromechanical power conversion"NewYork, Mc Graw-Hill (1966), chapter 7.

[4] M. Liwachitz-Garik and C.C. Whipple "Alternating current machines" D. Van Nostrand Co, Inc. Princeton, N J (1961).

[5] E. Rummich "linear synchronous Machines" Bull. A.S.E. 63(1972)23, 1 Nov, PP (1338-1344).

[6] J F Eastham "Linear machines, present status and future potential" Proc of the Conf. on Drives/Motors/Control 1985 July 15-17, London, England

[7] P.M Silson, "Modeling and control of a linear synchronous motor driven levitated vehicle" The Int. Conf. Publication No. 252 vol. 2, control 1985, Jul. 9-11 PP(540-544), Cambridge England.

[8] R.T Lipezynsk. "Linear synchronous motor control". IEE Power Div, colloquium (Digest) No. 1983/11, Publ. By IEE, London, England

[9] A.R Eastham, and others "Design and operation of the homopolar linear synchronous motor for linear drive and for integrated suspension/ propulsion application" Int. Conf. on Maglev Transport Now and for the furur 1984 Oct. 9-10

[10] G.E Dawson , A.R Eastham "Computer aided design studies of the Homopolar Linear Synchronous Motor". IEEE Trans on Mag. Vol. 20 No.5 Sep. 1984 Int. Magnetics Conf.

[11] J.F. Eastham "Novel synchronous machines linear and disc" IEE Proce Part B Vol. 137 No. 1 Jan. 1990 (p 49 - p 58)

[12] Mizuno, TsutomuYamada, Majime "Magnetic Circuit Analysis of a Linear Synchronous Motor with Permanent Magnets" Int. Magnetics Conf. 1992, IEEE Trans. On magnetics Vol. 28 No. 5 pt. 2 Sep. 1992 p(3027-3029)

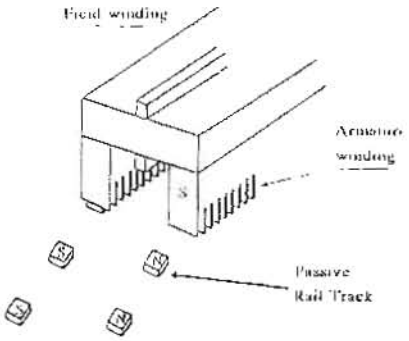

Fig. (1) Sketch of an idealized c-core Homopolar Linear Synchronous motor

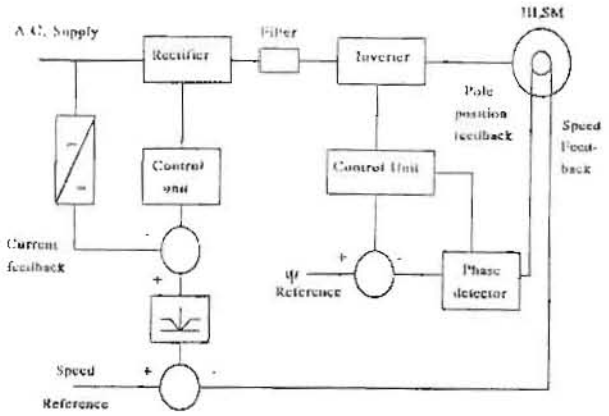

Fig. (2) Block diagram of a control system for the HLSM

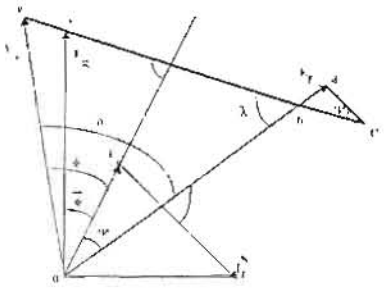

$$\overline{bd} = (X_{ad} - X_{aq})\, I_a \sin\psi$$

$$\overline{od} = E_f = I_f' X_{af}$$

$$\overline{ba} = X_{aq}\, I_a$$

$$\overline{ac} = X_{ad}\, I_a$$

$$\overline{ae} = X_l\, I_a$$

Fig. (3) Phasor diagram of voltage components for LSM (resistance neglected) with lagging current

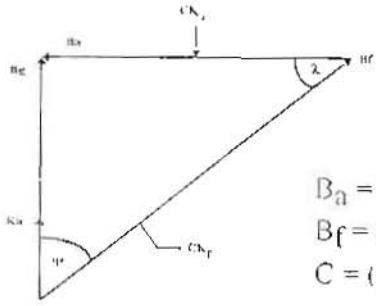

$$B_a = Ck_a$$

$$B_f = Ck_f$$

$$C = (\mu_0 \tau / \pi g)$$

Fig. (4) Phasor diagram for flux density components for ideal LSM

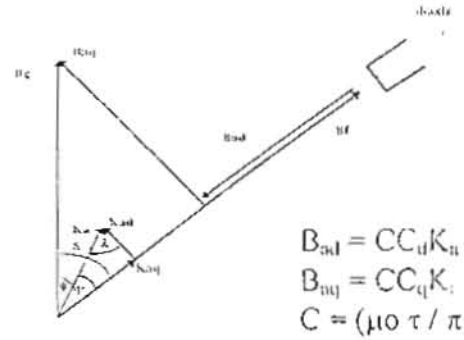

$$B_{ad} = CC_d K_a \sin\psi$$
$$B_{aq} = CC_q K_a \cos\psi$$
$$C = (\mu o\, \tau / \pi g)$$

Fig. (5) Phasor diagram for flux density components for LSM with lag. power factor

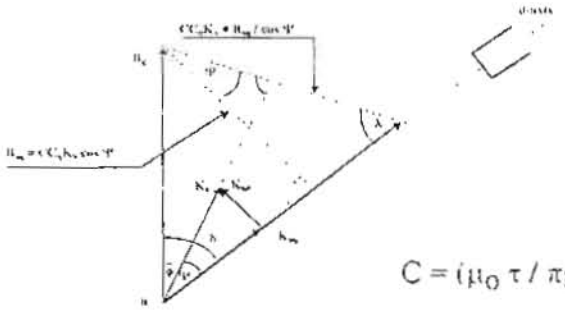

$$C = (\mu_o\, \tau / \pi g)$$

Fig. (6) Graphical construction used to determine the angle ψ

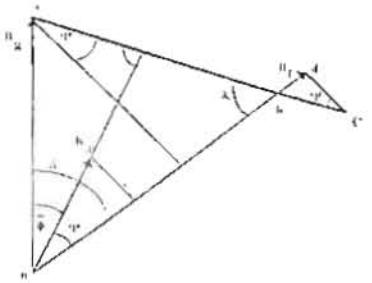

$$\overline{ac} = CC_d K_a$$
$$\overline{ab} = CC_q K_a$$
$$\overline{bd} = CK_a (C_d - C_q) \sin\psi$$
$$C = (\mu_o\, \tau / \pi g)$$

Fig. (7) Graphical construction used to determine B_f

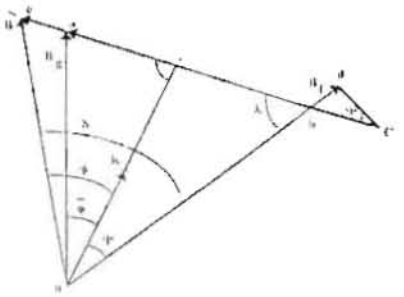

$$\overline{ac} = CC_d K_a = C_d B_a$$
$$\overline{ab} = CC_q K_a = C_q B_a$$
$$\overline{bd} = CK_a (C_d - C_q) \sin\psi$$
$$= B_a (C_d - C_q) \sin\psi$$
$$\overline{ae} = B_a (X_l / X_m)$$

Fig. (8) Phasor diagram accounting for leakage inductance
(Motor operating with lagging current)

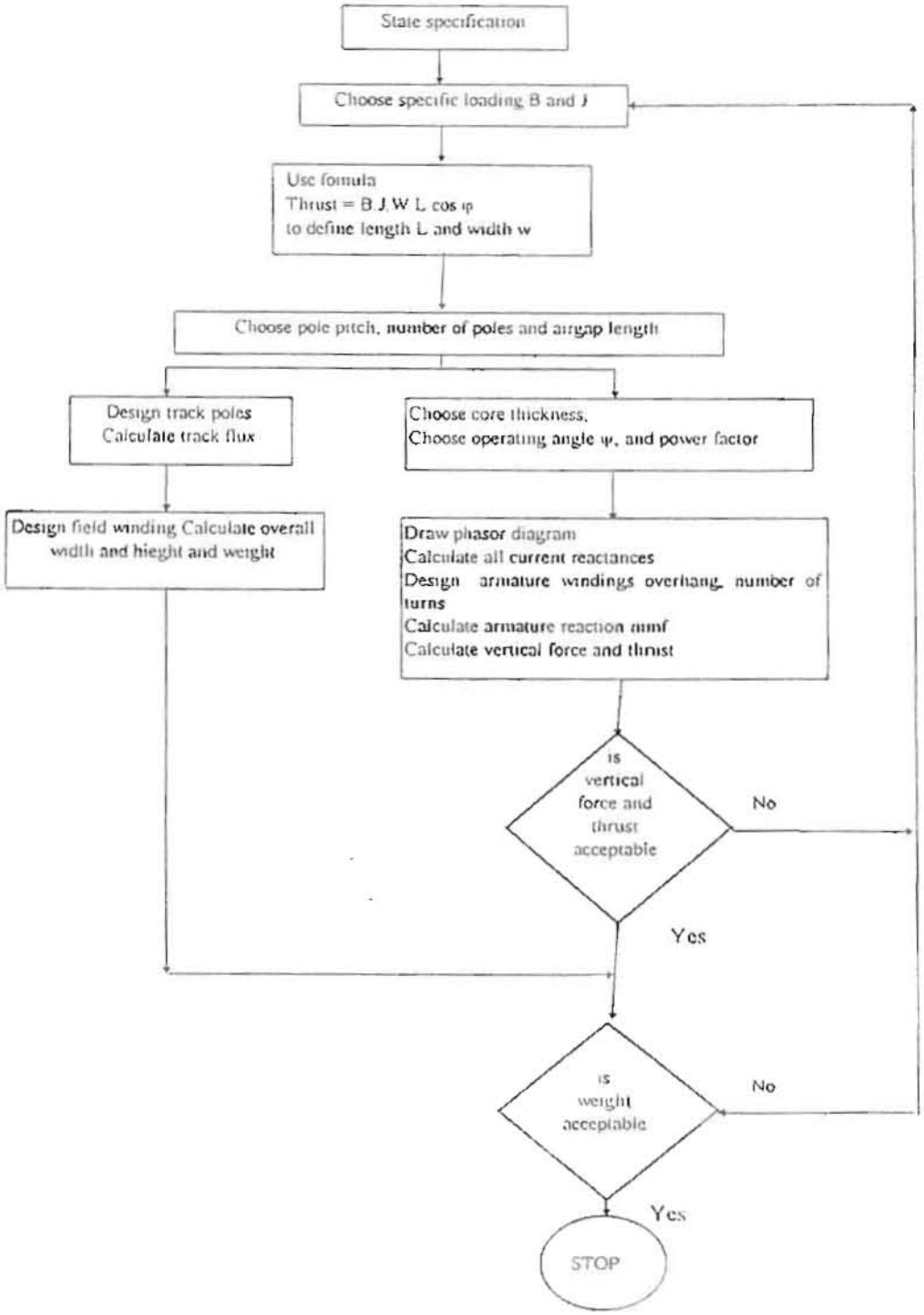

Fig. 9 : Flow chart of design process